Title
Effect of intra-myocardial Algisyl-LVR™ injectates on fibre structure in porcine heart failure

Authors
Sack, KL
Aliotta, E
Choy, JS
et al.

Publication Date
2018-11-01

DOI
10.1016/j.jmbbm.2018.07.005

Peer reviewed

HHS Public Access

Author manuscript

J Mech Behav Biomed Mater. Author manuscript; available in PMC 2018 November 21.

Published in final edited form as:

J Mech Behav Biomed Mater. 2018 November ; 87: 172–179. doi:10.1016/j.jmbbm.2018.07.005.

Effect of intra-myocardial Algisyl-LVR™ injectates on fibre structure in porcine heart failure

K.L. Sack[a,b], **E. Aliotta**[c], **J.S. Choy**[d], **D.B. Ennis**[c], **N.H. Davies**[a], **T. Franz**[a,e], **G.S. Kassab**[d], and **J.M. Guccione**[b,*]

[a]Division of Biomedical Engineering, Department of Human Biology, University of Cape Town, Cape Town, South Africa

[b]Department of Surgery, University of California at San Francisco, San Francisco, CA, USA

[c]Department of Radiological Sciences, University of California, Los Angeles, CA, USA

[d]California Medical Innovations Institute, Inc., San Diego, CA, USA

[e]Bioengineering Science Research Group, Engineering Sciences, Faculty of Engineering and the Environment, University of Southampton, Southampton, UK

Abstract

Recent preclinical trials have shown that alginate injections are a promising treatment for ischemic heart disease. Although improvements in heart function and global structure have been reported following alginate implants, the underlying structure is poorly understood. Using high resolution ex vivo MRI and DT-MRI of the hearts of normal control swine (n = 8), swine with induced heart failure (n = 5), and swine with heart failure and alginate injection treatment (n =6), we visualized and quantified the fibre distribution and implant material geometry. Our findings show that the alginate injectates form solid ellipsoids with a retention rate of 68.7% ± 21.3% (mean ± SD) and a sphericity index of 0.37 ± 0.03. These ellipsoidal shapes solidified predominantly at the mid-wall position with an inclination of −4.9° ± 31.4° relative to the local circumferential direction. Overall, the change to left ventricular wall thickness and myofiber orientation was minor and was associated with heart failure and not the presence of injectates. These results show that alginate injectates conform to the pre-existing tissue structure, likely expanding along directions of least resistance as mass is added to the injection sites. The alginate displaces the myocardial tissue predominantly in the longitudinal direction, causing minimal disruption to the surrounding myofiber orientations.

Keywords

Heart failure; Biomaterial injection therapy; Alginate; Diffusion tensor imaging; Myofiber orientation

*Correspondence to: Division of Adult Cardiothoracic Surgery, Department of Surgery, School of Medicine, UCSF, Mount Zion Harold Brunn Institute for Cardiovascular Research, 1657 Scott St., Room 219, San Francisco, CA 94143, USA. julius.guccione@ucsf.edu (J.M. Guccione).

1. Introduction

There is considerable interest in intra-myocardial biomaterial (e.g., alginate) injections as a treatment of myocardial infarction (MI) and infarct-induced heart failure (HF). Injectable biomaterials have shown promise in pre-clinical studies resulting in a range of improvements including increased ventricular wall thickness (Christman et al., 2004; Landa et al., 2008; Plotkin et al., 2014; Kadner et al., 2012; Dobner et al., 2009; Sabbah et al., 2013; Leor et al., 2009), increased scar thickness (Landa et al., 2008; Kadner et al., 2012; Leor et al., 2009), higher ejection fractions (Christman et al., 2004; Landa et al., 2008; Plotkin et al., 2014; Kadner et al., 2012; Sabbah et al., 2013) and decreased ventricular dilation (Christman et al., 2004; Landa et al., 2008; Plotkin et al., 2014; Kadner et al., 2012; Dobner et al., 2009; Sabbah et al., 2013; Leor et al., 2009). Alginate injections are known to have nonthrombogenic properties (Lee and Mooney, 2001; Cabrales et al., 2005) in addition to mitigating the effects of adverse ventricular remodelling following MI, which makes them a particularly viable potential therapy.

Human HF patients treated with Algisyl-LVR™, a commercialized injectable alginate polymer, and coronary-artery bypass-grafting showed dramatic improvements in ejection fraction, decreased ventricular wall stress, and increased wall thickness at 3 and 6 months post treatment (Lee et al., 2013a). Additionally, HF patients enrolled in clinical trials experienced significant improvement in New York Heart Association (NYHA) class description, mean peak VO_2 and quality of life (Lee et al., 2015; Mann et al., 2015). These studies all recognize the potential of Algisyl-LVR™ as an emerging therapy for HF and recommend further development and investigation in order to aid the development of a more effective (and potentially patient-specific) treatment.

The degree of efficacy likely depends on a range of factors, especially the local interactions between the alginate material and the surrounding tissue. The impact on the surrounding myofibre structure and the nature of myocardial tissue displacement is poorly understood. For example, the increased wall thickness reported in several studies has been ascribed to several causes, including radial displacement of the tissue, tissue growth, or possibly an inflammatory response to the foreign material (Nelson et al., 2011). A better understanding of the mechanical effect of the alginate injectates can more clearly identify the mechanisms responsible for the observed efficacy and assist with design of better treatment protocols to maximize clinical outcome. To aid this, we used Algisyl-LVR™ to treat HF in porcine subjects. Our recently published findings regarding the in vivo effects confirmed previous findings of increased ejection fraction, increased wall thickness in the infarcted region and reduction of stress (Choy et al., 2018). In a follow-up to that study, here we report on the ex vivo findings.

It is difficult to separate form and function in the in vivo heart. By quantifying the impact of Algisyl-LVR™ injections ex vivo, we provide objective and consistent measurements. This is achieved by investigating changes to regional myofibre orientations and global myocardial structure using ex vivo diffusion tensor magnetic resonance imaging (DT-MRI) techniques. DT-MRI is a well-established method for quantifying myofibre orientation (Holmes et al., 2000; Scollan et al., 1998) and the laminar structure (Helm et al., 2005; Kung

et al., 2011) from ex vivo myocardium. We also sought to quantify the retention rate and morphology of the alginate injectates in order to clarify the mechanism of action.

2. Materials and methods

Animals used in this study were treated under a protocol approved by the California Medical Innovations Institute's Institutional Animal Care and Use Committee and in compliance with the "Guide for the Care and Use of Laboratory Animals" prepared by the Institute of Laboratory Animal Resources, National Research Council, and published by the National Academy Press, revised 1996.

2.1. Experimental protocol

Eleven domestic swine with HF weighing 42.6 ± 1.9 kg and eight controls weighing 61.3 ± 13.4 kg were used in this study. The animals and subsequent data were divided into groups according to treatment as follows: Normal control (NC) subjects that served as a control (n = 8); Heart-failure injected (HFI) subjects that received biomaterial injections (n = 6), and heart-failure control (HFC) subjects that served as control (n = 5).

To induce HF, the obtuse marginal branches of the left circumflex artery were occluded in each animal. This was achieved via the percutaneous placement of embolization coils using a microcatheter (Cantata 2.9, Cook Medical, Bloomington, IN) to access the artery. Delivery of one to three 2- or 3-mm diameter embolization coils (depending on the anatomical variation) at two different time points (week 0 and week 2) resulted in ischemia and subsequent HF. The animals designated for treatment recovered for eight weeks before biomaterial injection therapy. The control animals recovered for sixteen weeks without biomaterial treatment. The experimental protocol for the HFI group is illustrated in Fig. 1.

The calcium-alginate biomaterial Algisyl-LVR™ (LoneStar Heart Inc. Laguna Hills, CA) used in this study has previously been described in detail (Lee et al., 2015). The separate material components are mixed immediately before use and then combined in one syringe for delivery as direct intramyocardial injections (Lee et al., 2013b). The polymer forms solid inclusions inside the myocardial wall and achieves its final material stiffness of 3–5 kPa.

Algisyl-LVR™ was directly injected in a circumferential pattern into the left ventricle (LV) free wall during an open chest procedure. A total of 12–14 injections (0.3 ml each) were administered in two rows: one above and one below the mid-ventricular plane between the base and the apex (from the anterior to the posterior wall). The injections were approximately 1.5 cm apart from each other. The animals were allowed to recover and were sacrificed eight weeks after the injection procedure. Excised hearts were fixed with buffered formalin (Carson-Millonig formulation).

2.2. Ex vivo imaging

After fixation, the left ventricular and atrial cavities were filled with a silicone rubber compound (Polyvinylsiloxane, Microsonic Inc., Ambridge, PA). The hearts were then placed in a plastic cylindrical container filled with a susceptibility-matched fluid (Fomblin, Solvay Solexis, West Deptford, NJ) and held in place using open-cell foam. Magnetic resonance

imaging (MRI) was then performed (Magnetom Prisma 3T, Siemens, Erlangen, Germany) with the following parameters: T1-weighted imaging using a 3D Fast Low Angle SHot (FLASH) sequence (0.3 × 0.3 × 0.8 mm spatial resolution, echo time (TE)/repetition time (TR) = 3.15 ms/12 ms, scan time: 1.5 h); and T2-weighted imaging using a 2D multi-slice Turbo Spin Echo (TSE) sequence (0.3 × 0.3 × 0.8 mm spatial resolution, TE/TR = 94 ms/15460 ms, scan time: 2 h).

DT-MRI was performed using a readout-segmented diffusion-weighted spin-echo sequence (Porter and Heidemann, 2009) with b-value = 1000 s/mm^2 along 30 directions and one b-value = 0 s/mm^2 reference, TE/TR = 62 ms/18100 ms and 1.0 × 1.0 × 1.0 mm spatial resolution with 4–6 signal averages to improve signal-to-noise ratio (SNR) (scan time: 8–12 h). Diffusion tensors were reconstructed from the diffusion weighted images using linear regression and custom Matlab (The MathWorks, Inc., Natick, Massachusetts, United States) routines.

2.3. Geometric segmentation and reconstruction

Ex vivo MRI data sets were imported and processed in Simpleware ScanIP (Synopsys, Mountain View, USA). Geometrically detailed segmentations of the LV were created along with segmentations of infarcted tissue and biomaterial injections when applicable. Segmentation relied on a combination of well-established techniques including region growing, level-set thresholding, and morphological smoothing (Setarehdan and Singh, 2012; Vadakkumpadan et al., 2010). Manual intervention was used only if needed to eliminate spurious features. In order to preserve the detailed features of the infarct morphology and overall volume, smoothing was not applied in the segmentation of the infarcted tissue. Finally, the LV was truncated at the base and partitioned into the 17 American Heart Association (AHA) regions (Cerqueira et al., 2002) to allow for a comparative analysis between animals. A complete diagram of the 17 AHA regions is provided in Fig. 2(a) and (b) for reference.

LV wall volume measurements were recorded from the segmentations to quantify the amount of healthy tissue, fibrotic tissue and biomaterial in each heart. LV surfaces were mapped to the image coordinate space for the MRI and DT-MRI data to enable a clear segmentation of imaging data bound only between these surfaces.

We introduced prolate spheroidal coordinates (Lombaert et al., 2012; Toussaint et al., 2013) into the image-coordinate space aligned with the long axis of the LV for each subject. The prolate spheroidal coordinates were used to describe relative myofibre orientations, determine mid-wall positions, measure wall thickness and accurately compare relative positions between subjects.

2.4. Myofibre orientation

DT-MRI provides diffusion tensors for each voxel that were de-composed into eigenvalues and corresponding eigenvectors. Primary eigenvectors associated with the largest eigenvalue were identified as the orientation of the myofibre (Holmes et al., 2000; Scollan et al., 1998; Kung et al., 2011). As illustrated in Fig. 2(c) and (d), myofibre orientation is decomposed into two angles:

1. α_h, the inclination angle, quantifies the angle between the myofibre projected onto the longitudinal-circumferential tangent plane and the circumferential unit vector.
2. α_t, the transverse angle, describes the angle between the myofibre projected onto the circumferential-radial tangent plane and the circumferential unit vector.

Angles were collected for each AHA region, and a relative radial position was recorded with endocardial surface = −1 and epicardial surface = +1. This allowed for easy quantification of myofibre orientation in reference to the local coordinates of the LV. In order to ensure only voxels containing cardiac tissue (and not gel, fat, air bubbles or voids) were included in the analysis of myofibre orientations, the requirements that eigenvalues of each voxel be strictly positive, and that the fractional anisotropy (FA), an invariant of diffusion tensors commonly used for tissue thresholding, is larger than 0.12, were imposed prior to analysis. This value for FA was found experimentally to be the lowest that would fully threshold out the gel and was reasonably different from values of FA for cardiac tissue (Helm et al., 2005; Kung et al., 2011; Wu et al., 2009).

Additionally, fibres that had large inclination angles (i.e., absolute value of αh exceeding 85°) were removed from the analysis of α_t. These vectors have little or no component in the radial plane, making their projections (when normalized) and subsequently their calculated angles highly distorted. Tractography (using DT-MRI software package suite AFNI (Taylor and Saad, 2013; Cox, 1996)) was also performed on the LVs to depict the myofibre structure surrounding gel injections.

2.5. Gel morphology and retention

The segmentation of the Algisyl-LVR™ injectates was analysed for geometric features. Retention rates were calculated from volume measurements of ex vivo segmentation and injected volumes recorded for each heart at the time of treatment. Additionally, ellipsoidal descriptions associated with each injectate were constructed whereby a 3D ellipsoid surface described by:

$$\frac{x^2}{a^2} + \frac{y^2}{b^2} + \frac{z^2}{c^2} = 1, \quad (1)$$

was fitted to each injectate surface using custom scripts (MATLAB and the Optimization Toolbox 2012b). Orientation, sphericity, and radial position of the fitted ellipsoids were assessed. Ellipsoid orientation followed the same approach as for myofibre orientation, i.e., inclination and transverse angle where the ellipsoid's long-axis served as reference. Values were quantified for each injectate and averaged over a single heart or entire group, as appropriate.

2.6. Statistical analysis

Data in this study are expressed as mean ± SD unless otherwise stated. The differences between the various groups were evaluated using analysis of variance (ANOVA) and Student's t-test. The differences were considered statistically significant at $p < 0.05$.

3. Results

3.1. Volume and thickness measurements

The mean LV wall volume was 119.6 ± 46.0 ml, 142.7 ± 29.5 ml, and 134.0 ± 29.3 ml, for the NC, HFC and HFI group, respectively. The mean volume fraction of biomaterial, infarcted tissue and healthy tissue was 1.9%, 7.8% and 90.3%, respectively, for the HFI group and 0%, 8.6% and 91.4%, respectively, for the HFC group. The results for each heart are presented in Table 1.

Wall thickness was measured from a minimum of 1800 data points for each LV and means were calculated for each AHA region to provide regional thickness values for each subject. Each subject's regional mean values were used to obtain group regional mean values shown in Fig. 3. The group mean wall thickness for the unloaded ex vivo LV was found to be very similar between groups, i.e. 17.9 ± 3.4 mm for NC, 18.2 ± 3.6 mm for HFC, and 18.3 ± 2.1 mm for HFI (no statistical significance, n.s.). The only significant difference between groups was found in AHA region 6, where wall thickness of the NC (19.6 ± 2.1 mm) was substantially larger than that of the HFC (16.7 ± 2.8 mm) and the HFI (16.5 ± 2.3 mm) ($p < 0.05$).

3.2. Myofibre orientation

The inclination fibre angles αh in each group are presented in Fig. 4 for LV free wall AHA regions 1, 4, 5, 6, 7, 10, 11 and 12, which are most likely to contain injectates. Inclination angles α_h are similar across groups, with a difference of 13.9° ± 10.0° (NC versus HFC) and 12.5° ± 10.4° (NC versus HFI) (n.s.).

The transverse fibre angles αt for each group are presented in Fig. 5 for the same LV free wall regions used for α_h. The regional mean values of α_t are close to 0° throughout the LV. The LV mean of αt are −5.3° ± 28° (NC), −2.8° ± 31° (HFC), and −2.3° ± 31° (HFI). Differences of αt between groups were even smaller than those for α_h, namely 8.7° ± 6.0° (NC versus HFC) and 6.9° ± 5.8° (NC versus HFI) (n.s.).

The myofibre orientation surrounding an injectate is shown in Fig. 6, whereby tractography was used surrounding a short-axis image of an LV with a prominent injectate. Tracts displayed are only those that pass through a selected prism that isolates specific myofibre pathways. Tightly grouped myofibre tracts diverge near the injectate and pass the injectate longitudinally above and below Fig. 6(b), whereas there is no visual evidence of radial deflection of the myofibres (Fig. 6(c)). Online supplementary animations, which rotate the viewpoint around the Algisyl-LVR™ injectate, illustrate this point more clearly.

3.3. Injectate morphology

Many of the injectates exhibited an ellipsoidal shape. The volumetric retention of injected material was 68.7% ± 21.3%. The mean injectate dimensions were 1.9 mm, 2.9 mm and 7.1 mm along the three ellipsoidal axes. This resulted in a sphericity index (ratio of mean of short axes to long axis) of 0.37 ± 0.03. The injectates were located roughly mid-wall (between endocardial and epicardial surfaces) with the injectates' centre of mass found at normalized wall-depth co-ordinates of 0.28 ± 0.08. Individual subject results are presented in Table 2.

The ellipsoid (long axis) inclination angle was −4.9° ± 31.35°. The distribution of these results is shown in Fig. 7(a). Injectates with sphericity index > 0.5 were assumed unable to form properly in situ and treated as outliers (also identified in Fig. 7(b)). Excluding outliers, the ellipsoid inclination angle and myofibre inclination angle of the surrounding tissue correlate with $R = 0.59$ ($p < 0.01$); see also Fig. 7(b). A typical arrangement of injectates in the myocardial wall is shown in Fig. 8(a) and (b). Close up views in Fig. 8(c) and (d) reveal the complex morphology of the injectates.

4. Discussion

To the best of our knowledge, this study is the first to report the quantitative impact of intra-myocardial biomaterial injectates on the structure of the surrounding tissue in swine hearts with HF. In addition to quantifying the retention rate and morphology of the injectates we found that differences in myofibre orientation from the normal case were present in both the HFC and HFI subjects, albeit these differences were slightly smaller in the treated subjects.

The mean myofibre orientation observed for normal control swine serves as a validation of our methods because the results agree well with those in other studies using large animal models (Helm et al., 2005; Streeter et al., 1969; Nielsen et al., 1991; Streeter and Bassett, 1966; Ennis et al., 2008; Geerts et al., 2002) and previous regional DT-MRI myofibre analysis reported similar SDs (Scollan et al., 1998; Lombaert et al., 2012).

We compared the HFI group to the HFC and NC groups to examine the effects of the Algisyl-LVR™ injectates on myofibre orientation. Lower values of the myofibre inclination angle α_h in regions containing infarction (particularly the anterolateral region AHA 6) are consistent with values reported in other studies (Wu et al., 2009, 2007). No significant difference in α_h resulting from Algisyl-LVR™ injectates was observed in HFI subjects. Furthermore, the similarity in the degree that α_h differs between the NC and the HF groups implies that HF, and not the injected material, is responsible for these changes.

The differences for the transverse myofibre angle α_t between both the HFC and the HFI groups and the NC group were even smaller than those for the myofibre inclination angle. The negligible effect of the Algisyl-LVR™ injectates on α_t indicates that radial displacement of tissue due to the biomaterial injection is minimal, and tissue volume is displaced predominantly longitudinally. This can be seen qualitatively in the visualization of myofibre tracts in Fig. 6 (and supplementary videos), which show the fibre pathways diverted above and below the injectate in the longitudinal direction with no disturbance of

fibre pathways in the radial direction (Supplementary material related to this article can be found online at doi:10.1016/j.jmbbm.2018.07.005).

In swine with HF, the smaller changes in fibre orientation in those that received Algisyl-LVR™ injections than in those who did not, namely $\Delta\alpha_h$ 12.5° vs. 13.9° and $\Delta\alpha_t$ 6.9° vs. 8.7°, indicates a beneficial overall effect of the injections on myofibre orientations in the failing heart. The exact mechanism of action is unclear, but we hypothesize that the long-term presence of Algisyl-LVR™ injectates anchors the surrounding fibre structure, thereby mitigating further adverse remodelling. This an-choring could be achieved via a previously reported finding that the alginate material always induced a full encapsulation with fibrotic tissue (Sabbah et al., 2013; Choy et al., 2018).

The Algisyl-LVR™ injectates conformed to the surrounding myocardial structure such that the long axis of the ellipsoidal injectates were typically aligned in a circumferential direction (Fig. 7), which accords with the local myofibre direction at the mid-wall (approximate site of injection). We propose this particular alignment results from liquid Algisyl-LVR™ initially displacing interstitial fluid and subsequently separating myocardium along cleavage planes of least resistance during the injection process.

Achieving high retention for injected material into the heart is challenging given the significant motion and perfusion of the heart (i.e., some of the material may be removed through the coronary venous system). The observed retention rate in this study of 68.7% is considered high compared with rates reported in other studies (Al Kindi et al., 2008; Malliaras et al., 2011; Roche et al., 2014). It should be noted that sometimes the injections seem to have merged during the injection process, which results in fewer injectates than injections (see Table 1 and Fig. 8).

An increase in wall thickness due to alginate injectates is not seen in the measurements of ex vivo unloaded hearts. The visualization of myofibre tracts in Fig. 6 (and supplementary videos) provides further support for the preserved wall thickness after injections. As can be seen, a large injectate occupies more than half of the LV wall thickness without creating any bulging on the epicardial or endocardial surface. This finding is at odds with our own in vivo measurements of the same subjects (Choy et al., 2018) and multiple studies that found increases in wall thickness due to biomaterial injection therapy (Christman et al., 2004; Landa et al., 2008; Plotkin et al., 2014; Kadner et al., 2012; Dobner et al., 2009; Sabbah et al., 2013; Leor et al., 2009). These differences in in vivo and ex vivo findings may reveal an important mechanism of the treatment. As these in vivo findings typically measure wall thickness at end-dia-stole, which had considerably lower cavity pressures in the treated cohorts, we can infer that these gains in wall thickness are likely due ventricular unloading. In other words, treated subjects experience more favourable pressure conditions in vivo, which directly influences in vivo measurements of wall thickness. This would explain the lack of change in wall thickness when all hearts are in an unloaded state. A quick calculation accounting for the retained volume of the injectates (2.5 ml on average) and the endocardial surface area in humans (60–140 cm^2 (Gopal et al., 1993)) shows that, even under the most generous conditions, biomaterial injections could only add 0.4 mm in wall thickness. Ventricular unloading is a well-established method to mitigate, or in some cases reverse,

adverse remodelling effects of HF and is typically introduced via mechanical ventricular assistance devices (Birks et al., 2006; Burkhoff et al., 2006; Wohlschlaeger et al., 2005). Here biopolymer treatment appears to slow or mitigate the effects of adverse remodelling, which in turn improve cardiac performance, i.e. increased stroke volume and ejection fraction (Choy et al., 2018), which unloads the LV compared to untreated subjects.

Future work should focus on testing the hypothesis that the fibrotic encapsulation of the alginate material anchors the surrounding tissue and subsequently mitigates the chronic adverse remodelling effects due to HF. To confirm this, we plan to bind dexamethasone to our polymer to potentially reduce the fibrotic tissue response. A comparison of outcomes from subjects injected with biopolymer with and without a slow-release of dexamethasone will provide clarity on this hypothesis.

5. Conclusions

Our study demonstrated that swine with HF treated with Algisyl-LVR™ displayed similar, albeit slightly more normal, myofibre orientations compared to HF swine without treatment. The minimal interference of Algisyl-LVR™ injectates with the myocardial structure can be interpreted as an additional assurance of treatment safety. Our most interesting finding was the similarity of wall thickness between treated and untreated subjects measured ex vivo. In recently published research of the exact same animals, we showed how the in vivo measured wall thickness between these groups was different. The combination of these findings indicates that the treated subjects experience unloading benefits due to therapy, that the biopolymer injections change the trajectory of HF and that these create cascading benefits (i.e. a positive mechanical feedback loop), which are noticeable within 8 weeks of treatment. Finally, this study provides comprehensive data for the development of predictive computational models for the further advancement of biomaterial injection therapies in the heart.

Supplementary Material

Refer to Web version on PubMed Central for supplementary material.

Acknowledgements

This work was supported by NIH grants R01-HL-077921, R01-HL-118627 and U01-HL-119578. Further financial support was provided by the Oppenheimer Memorial Trust (OMT) and the National Research Foundation (NRF) of South Africa (UID 92531). Opinions expressed and conclusions arrived at, are those of the authors and are not necessarily to be attributed to the NRF or OMT.

References

Al Kindi A, et al., 2008 Cellular cardiomyoplasty: routes of cell delivery and retention. Front. Biosci 13, 2421–2434. [PubMed: 17981723]

Birks EJ, et al., 2006 Left ventricular assist device and drug therapy for the reversal of heart failure. N. Engl. J. Med 355 (18), 1873–1884. [PubMed: 17079761]

Burkhoff D, Klotz S, Mancini DM, 2006 LVAD-induced reverse remodeling: basic and clinical implications for myocardial recovery. J. Card. Fail 12 (3), 227–239. [PubMed: 16624689]

Cabrales P, Tsai AG, Intaglietta M, 2005 Alginate plasma expander maintains perfusion and plasma viscosity during extreme hemodilution. Am. J. Physiol.-Heart Circ. Physiol 288 (4), H1708–H1716. [PubMed: 15591096]

Cerqueira MD, et al., 2002 Standardized myocardial segmentation and nomenclature for tomographic imaging of the heart – a statement for healthcare professionals from the Cardiac Imaging Committee of the Council on Clinical Cardiology of the American Heart Association. Circulation 105 (4), 539–542. [PubMed: 11815441]

Choy JS, et al., 2018 Efficacy of intramyocardial injection of Algisyl-LVR for the treatment of ischemic heart failure in swine. Int. J. Cardiol 255, 129–135. [PubMed: 29425550]

Christman KL, et al., 2004 Fibrin glue alone and skeletal myoblasts in a fibrin scaffold preserve cardiac function after myocardial infarction. Tissue Eng. 10 (3–4), 403–409. [PubMed: 15165457]

Cox RW, 1996 AFNI: software for analysis and visualization of functional magnetic resonance neuroimages. Comput. Biomed. Res 29 (3), 162–173. [PubMed: 8812068]

Dobner S, et al., 2009 A synthetic non-degradable polyethylene glycol hydrogel retards adverse post-infarct left ventricular remodeling. J. Card. Fail 15 (7), 629–636. [PubMed: 19700140]

Ennis DB, et al., 2008 Myofiber angle distributions in the ovine left ventricle do not conform to computationally optimized predictions. J. Biomech 41 (15), 3219–3224. [PubMed: 18805536]

Geerts L, et al., 2002 Characterization of the normal cardiac myofiber field in goat measured with MR-diffusion tensor imaging. Am. J. Physiol. Heart Circ. Physiol 283 (1), H139–H145. [PubMed: 12063284]

Gopal AS, et al., 1993 Left ventricular volume and endocardial surface area by threedimensional echocardiography: comparison with two-dimensional echocardiography and nuclear magnetic resonance imaging in normal subjects. J. Am. Coll. Cardiol 22 (1), 258–270. [PubMed: 8509549]

Helm PA, et al., 2005 Ex vivo 3D diffusion tensor imaging and quantification of cardiac laminar structure. Magn. Reson. Med 54 (4), 850–859. [PubMed: 16149057]

Holmes AA, Scollan D, Winslow RL, 2000 Direct histological validation of diffusion tensor MRI in formaldehyde-fixed myocardium. Magn. Reson. Med 44 (1), 157–161. [PubMed: 10893534]

Kadner K, et al., 2012 The beneficial effects of deferred delivery on the efficiency of hydrogel therapy post myocardial infarction. Biomaterials 33 (7), 2060–2066. [PubMed: 22153866]

Kung GL, et al., 2011 The presence of two local myocardial sheet populations confirmed by diffusion tensor MRI and histological validation. J. Magn. Reson. Imaging 34 (5), 1080–1091. [PubMed: 21932362]

Landa N, et al., 2008 Effect of injectable alginate implant on cardiac remodeling and function after recent and old infarcts in rat. Circulation 117 (11), 1388–1396. [PubMed: 18316487]

Lee KY, Mooney DJ, 2001 Hydrogels for tissue engineering. Chem. Rev 101 (7), 1869–1880. [PubMed: 11710233]

Lee LC, et al., 2013a Algisyl-LVR with coronary artery bypass grafting reduces left ventricular wall stress and improves function in the failing human heart. Int. J. Cardiol 168 (3), 2022–2028. [PubMed: 23394895]

Lee LC, et al., 2013b Reduction in left ventricular wall stress and improvement in function in failing hearts using Algisyl-LVR. JoVE (J. Vis. Exp.)(74) (e50096–e50096).

Lee RJ, et al., 2015 The feasibility and safety of Algisyl-LVR™ as a method of left ventricular augmentation in patients with dilated cardiomyopathy: initial first in man clinical results. Int. J. Cardiol 199, 18–24. [PubMed: 26173169]

Leor J, et al., 2009 Intracoronary injection of in situ forming alginate hydrogel reverses left ventricular remodeling after myocardial infarction in Swine. J. Am. Coll. Cardiol 54 (11), 1014–1023. [PubMed: 19729119]

Lombaert H, et al., 2012 Human atlas of the cardiac fiber architecture: study on a healthy population. IEEE Trans. Med. Imaging 31 (7), 1436–1447. [PubMed: 22481815]

Malliaras K, Kreke M, Marban E, 2011 The stuttering progress of cell therapy for heart disease. Clin. Pharmacol. Ther 90 (4), 532–541. [PubMed: 21900888]

Mann DL, et al., 2015 One-year follow-up results from AUGMENT-HF: a multicentre randomized controlled clinical trial of the efficacy of left ventricular augmentation with Algisyl in the treatment of heart failure. Eur. J. Heart Fail.

Nelson DM, et al., 2011 Intra-myocardial biomaterial injection therapy in the treatment of heart failure: materials, outcomes and challenges. Acta Biomater. 7 (1), 1–15. [PubMed: 20619368]

Nielsen PM, et al., 1991 Mathematical model of geometry and fibrous structure of the heart. Am. J. Physiol 260 (4 Pt 2), H1365–H1378. [PubMed: 2012234]

Plotkin M, et al., 2014 The effect of matrix stiffness of injectable hydrogels on the preservation of cardiac function after a heart attack. Biomaterials 35 (5), 1429–1438. [PubMed: 24268664]

Porter DA, Heidemann RM, 2009 High resolution diffusion-weighted imaging using readout-segmented echo-planar imaging, parallel imaging and a two-dimensional navigator-based reacquisition. Magn. Reson. Med 62 (2), 468–475. [PubMed: 19449372]

Roche ET, et al., 2014 Comparison of biomaterial delivery vehicles for improving acute retention of stem cells in the infarcted heart. Biomaterials 35 (25), 6850–6858. [PubMed: 24862441]

Sabbah HN, et al., 2013 Augmentation of left ventricular wall thickness with alginate hydrogel implants improves left ventricular function and prevents progressive remodeling in dogs with chronic heart failure. JACC: Heart Fail. 1 (3), 252–258. [PubMed: 23998003]

Scollan DF, et al., 1998 Histological validation of myocardial microstructure obtained from diffusion tensor magnetic resonance imaging. Am. J. Physiol 275 (6 Pt 2), H2308–H2318. [PubMed: 9843833]

Setarehdan SK, Singh S, 2012 Advanced Algorithmic Approaches To Medical Image Segmentation: State-of-the-Art Applications In Cardiology, Neurology, Mammography And Pathology. Springer Science & Business Media.

Streeter DD, et al., 1969 Fiber orientation in the canine left ventricle during diastole and systole. Circ. Res 24 (3), 339–347. [PubMed: 5766515]

Streeter DD, Bassett DL, 1966 An engineering analysis of myocardial fiber orientation in pig's left ventricle in systole. Anat. Rec 155 (4), 503–511.

Taylor PA, Saad ZS, 2013 FATCAT:(an efficient) functional and tractographic connectivity analysis toolbox. Brain Connect. 3 (5), 523–535. [PubMed: 23980912]

Toussaint N, et al., 2013 In vivo human cardiac fibre architecture estimation using shape-based diffusion tensor processing. Med. Image Anal 17 (8), 1243–1255. [PubMed: 23523287]

Vadakkumpadan F, et al., 2010 Image-based models of cardiac structure in health and disease. Wiley Interdiscip. Rev.-Syst. Biol. Med 2 (4), 489–506.

Wohlschlaeger J, et al., 2005 Reverse remodeling following insertion of left ventricular assist devices (LVAD): a review of the morphological and molecular changes.Cardiovasc. Res 68 (3), 376–386. [PubMed: 16024006]

Wu EX, et al., 2007 MR diffusion tensor imaging study of postinfarct myocardium structural remodeling in a porcine model. Magn. Reson. Med 58 (4), 687–695. [PubMed: 17899595]

Wu Y, et al., 2009 MR study of the effect of infarct size and location on left ventricular functional and microstructural alterations in porcine models. J. Magn. Reson.Imaging 29 (2), 305–312. [PubMed: 19161181]

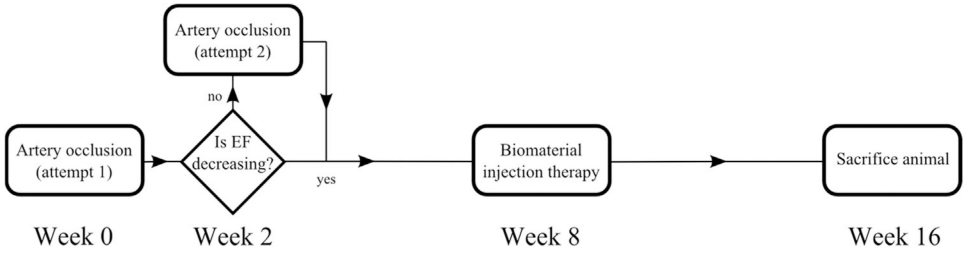

Fig. 1.

Schematic illustrating the experimental protocol for the HFI group. The HFC group received the same protocol treatment for weeks 0, 2 and 16 (i.e. excluding the biomaterial injection therapy).

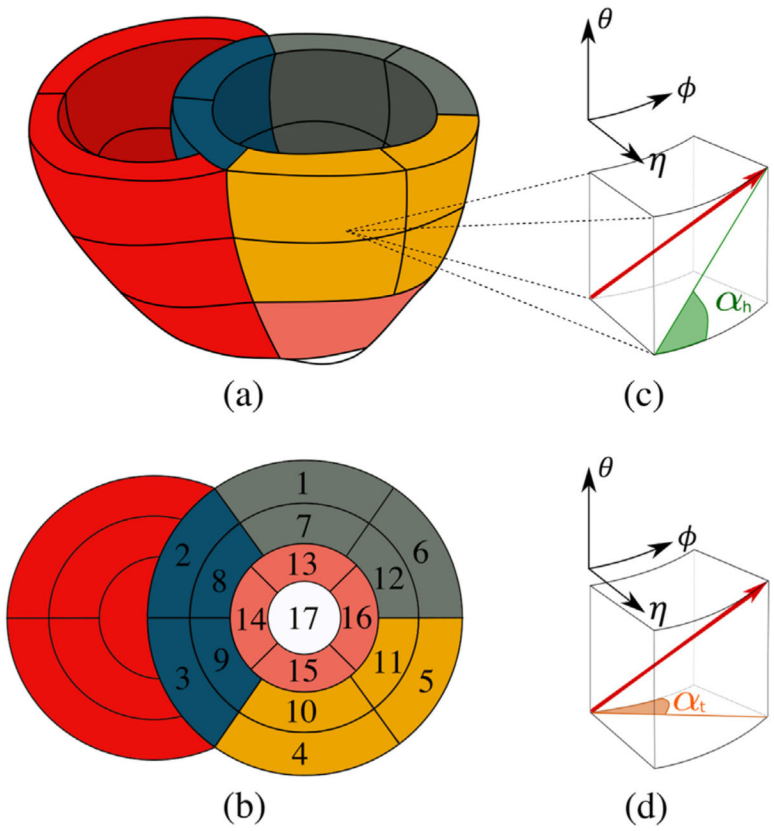

Fig. 2.

(a) Biventricular geometry with the LV partitioned into the 17 AHA regions. Regions are given distinct colours for ease of identification. (b) AHA labels that correspond to subfigure (a). AHA regions 1–6 partition the LV base, AHA regions 7–12 partition the LV mid-section and AHA regions 13–17 partition the LV apex. (c) The primary eigenvector (red arrow) is projected on the longitudinal-circumferential tangent plane (green line). The inclination angle αh is quantified by measuring the angle between this projection and the circumferential unit vector. (d) The primary eigenvector (red arrow) is projected on the circumferential-radial tangent plane (orange line). The transverse angle αt is quantified by measuring the angle between this projection and the circumferential unit vector. The triad of the local prolate spheroidal coordinate system is provided above subfigures (c–d). (For interpretation of the references to color in this figure legend, the reader is referred to the web version of this article.)

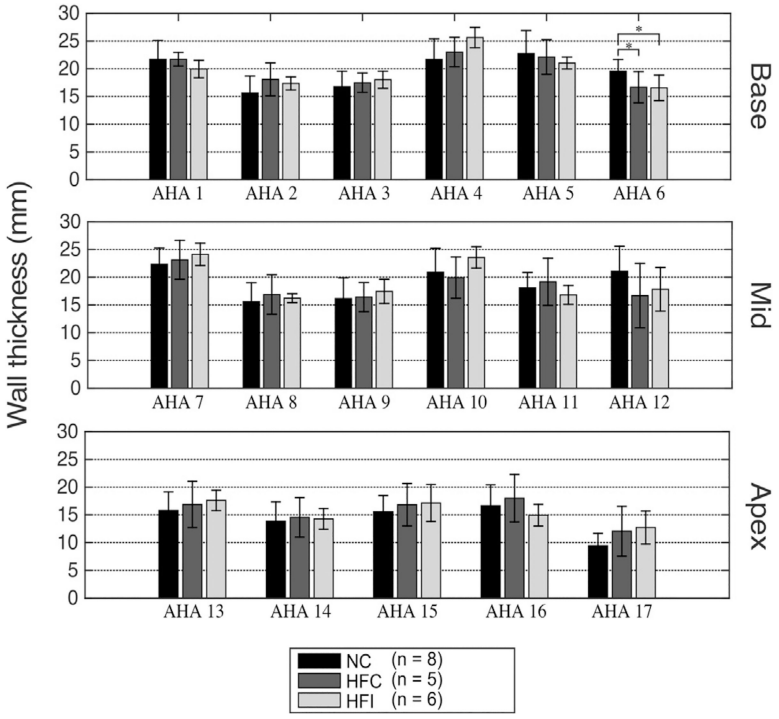

Fig. 3.

Mean wall thickness and standard of deviation for each of the 17 AHA regions for each group. Regions are presented in separate rows for each longitudinal section. * $p < 0.05$.

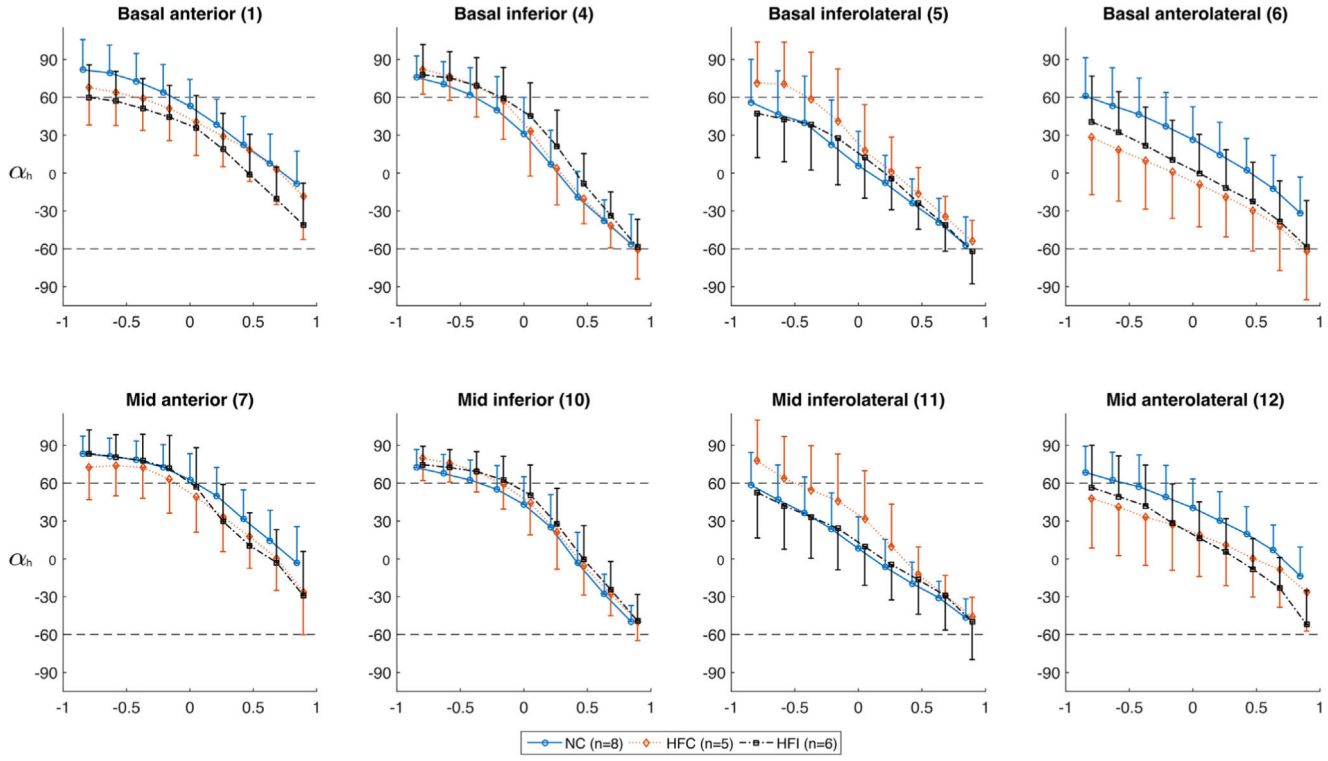

Fig. 4.

Inclination angles αh in each group for the LV free wall regions showing the distribution along the radial depth. The AHA region number is given in parenthesis after each subtitle. Normalized radial coordinates were used to indicated the endocardium (−1), mid wall (0) and epicardium positions (+1). Standard deviations for each group are presented in one direction only for visual clarity. Dashed lines corresponding to +60° and −60° are plotted for ease of comparison and because a significant number of studies use these bounds when prescribing α_h in LV computational models.

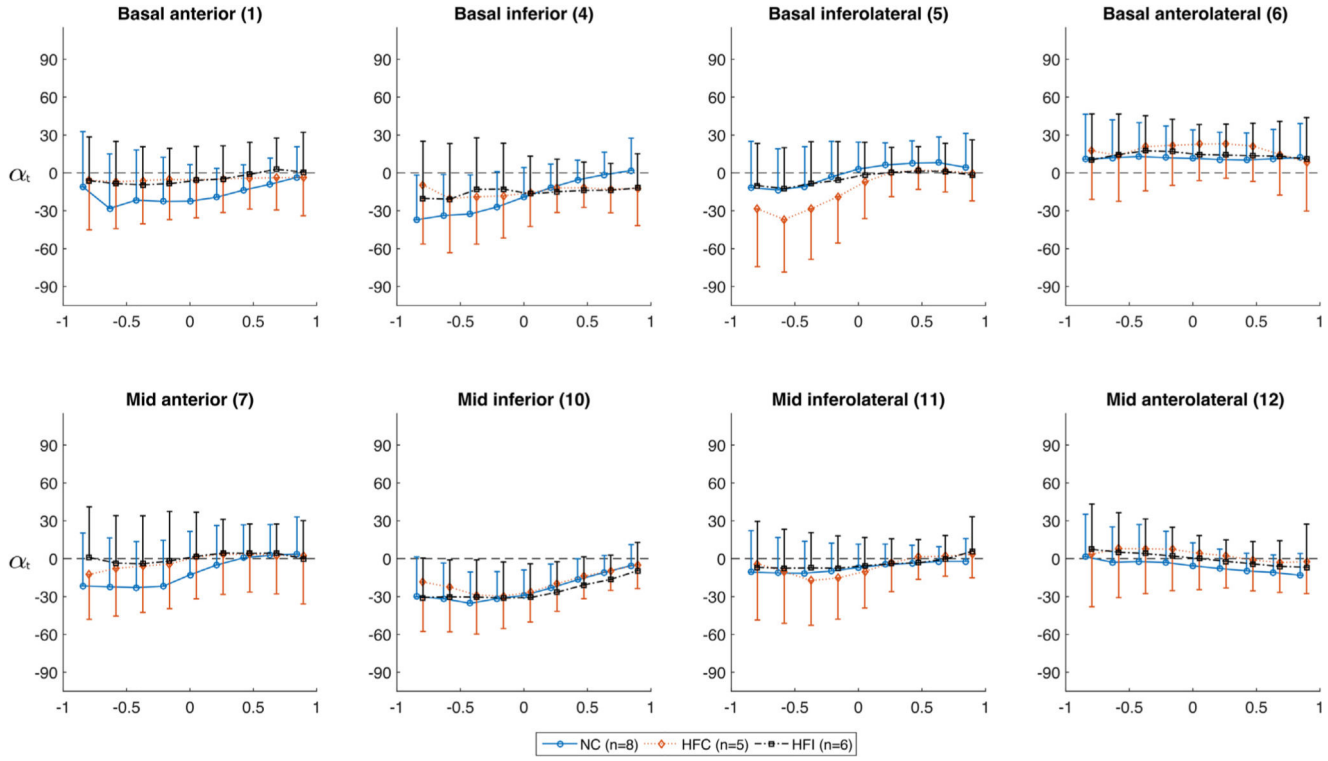

Fig. 5.

Transverse angles α_t in each group for the LV free wall regions showing the distribution along the radial depth. The AHA region number is given in parenthesis after each subtitle. Normalized radial coordinates were used to indicate the endocardium (−1), mid wall (0) and epicardium positions (+1). Standard deviations for each group are presented in one direction only for visual clarity. A dashed line at 0° is plotted for ease of comparison.

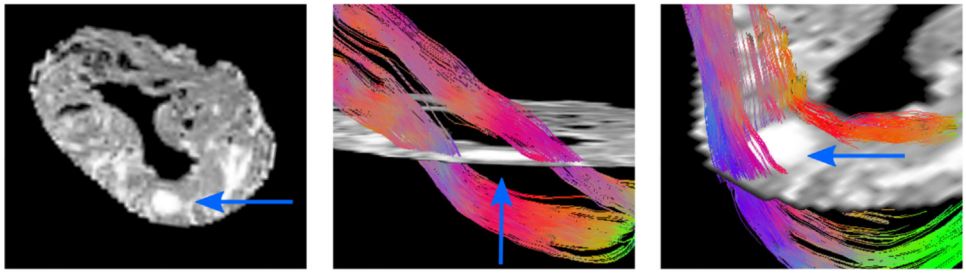

Fig. 6.

(a) A short axis slice for an LV region containing a prominent alginate injectate (blue arrow). (b) Selected tractography applied to the same short axis image in (a). Myofibre tracts displayed are only those that pass through a prism, with dimensions in mm for (x, y, z) as (1,1,6), which isolates myofibre tracts that pass longitudinally above and below a prominent alginate injectate (blue arrow). (c) Similar to (b), except the prism dimensions are (2,6,1) mm in order to isolate myofibre tracts that pass between the injectate and the epi-and endocardium walls. (For interpretation of the references to color in this figure legend, the reader is referred to the web version of this article.)

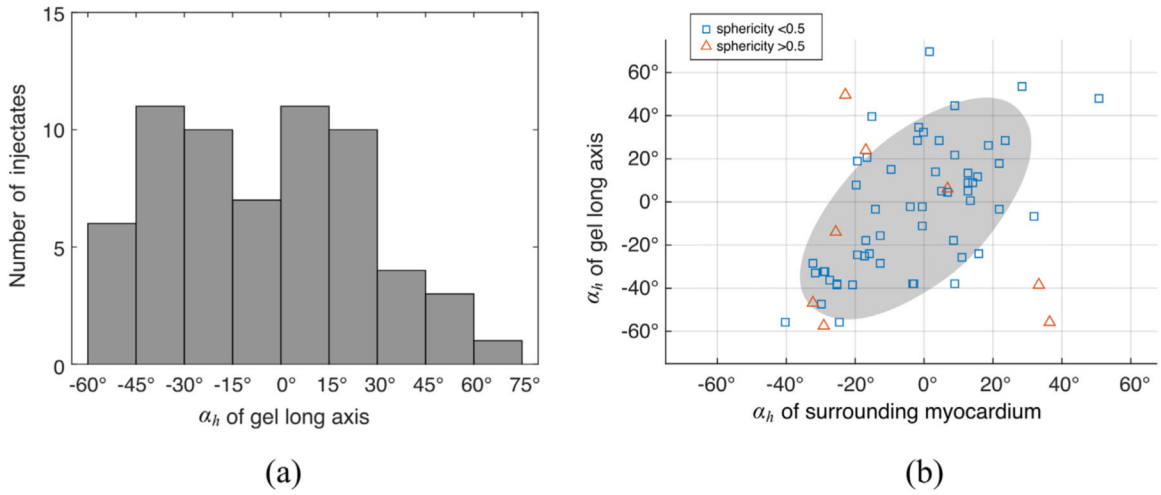

Fig. 7.

(a) The distribution of αh measured from the long-axis of the alginate injectate ellipsoids. Histogram bins have a width of 15°. (b) A scatter plot of the inclination angle of the injectate ellipsoids plotted against the inclination angle of the surrounding myocardium. Data were divided into two groups based on sphericity. We assumed that injectates unable to form properly would present as outliers and these could be isolated by a high sphericity (> 0.5). An ellipsoid silhouette displayed under the data indicates the 99% confidence region found from the data, assuming a Gaussian distribution.

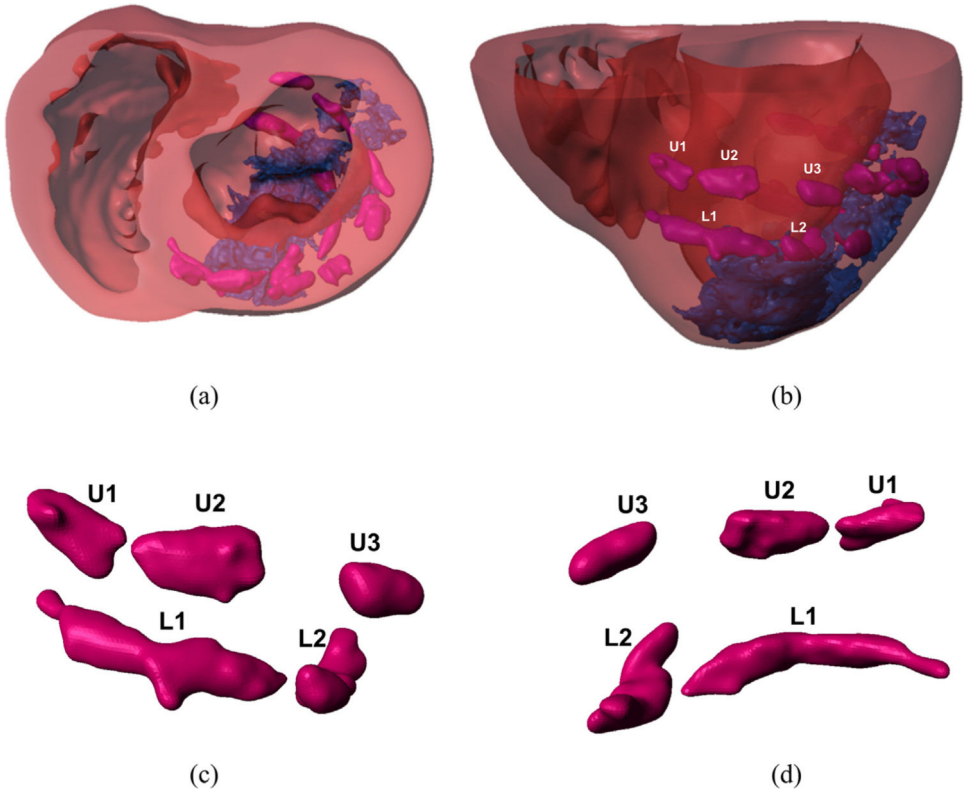

Fig. 8.

(a) Base-to-apex view of the truncated biventricular structure (red) of a porcine subject with MI (blue), revealing a typical injection pattern of Algisyl-LVR™ injectates (pink). (b) Anterior view of the same structure with injectates labelled according to their position in the upper (U) and lower (L) rows and circumferential position (1,2,3…). (c)–(d) Anterior and posterior close up views of the labelled Algisyl-LVR™ injectates revealing the complex (and sometimes merged) morphology. (For interpretation of the references to color in this figure legend, the reader is referred to the web version of this article.)

Table 1

Volume and volume fraction measurements for the individual hearts in the HFI and HFC groups.

Subject	Algisyl-LVR vol. (ml)	Infarcted tissue vol. (ml)	Total LV wall vol. (ml)	Algisyl-LVR vol. fr. (%)	Infarcted tissue vol. fr. (%)	Healthy tissue vol. fr. (%)
HFI 1	3.5	14.7	172.7	2.0	8.5	89.5
HFI 2	1.6	12.2	97.3	1.6	12.5	85.8
HFI 3	3.1	4.5	104.3	2.9	4.3	92.8
HFI 4	2.8	12.9	129.9	2.2	9.9	87.9
HFI 5	1.5	9.0	153.9	0.9	5.9	93.2
HFI 6	2.7	8.1	145.9	1.8	5.5	92.6
Mean ± SD	**2.5 ± 0.8**	**10.2 ± 3.7**	**134.0 ± 29.3**	**1.9 ± 0.7**	**7.8 ± 3.1**	**90.3 ± 3.0**
HFC 1	–	11.8	123.6	–	9.5	90.5
HFC 2	–	12.3	108.6	–	11.3	88.7
HFC 3	–	16.3	137.7	–	11.9	88.1
HFC 4	–	12.1	183.0	–	6.6	93.4
HFC 5	–	6.3	160.4	–	3.9	96.1
Mean ± SD	**0**	**11.8 ± 3.6**	**142.7 ± 29.5**		**8.6 ± 3.3**	**91.4 ± 3.3**

Abbreviations: vol., volume; fr., fraction.

Table 2

Basic parameters quantifying the retention and morphology of the alginate injectates.

Animal #	Injections delivered	Injections identified	Volume (ml)	Retention rate (%)	Wall depth	Sphericity
HFI 1	13	13	3.5	91	0.37	0.33
HFI 2	12	10	1.6	44	0.38	0.35
HFI 3	12	10	3.1	85	0.20	0.40
HFI 4	12	11	2.8	78	0.30	0.40
HFI 5	12	8	1.5	40	0.24	0.39
HFI 6	12	11	2.7	74	0.18	0.38
Mean ± SD				68.7 ± 21.3	0.28 ± 0.08	0.37 ± 0.03

Wall depth is reported using normalized coordinates, whereby −1 is associated with the endocardium and +1 with the epicardium.